Raman Spectroscopy Study and First-Principles Calculations of the Interaction between Nucleic Acid Bases and Carbon Nanotubes

Stepan G. Stepanian,*,† Maksym V. Karachevtsev,† Alexander Yu. Glamazda,† Victor A. Karachevtsev,† and L. Adamowicz‡

B. Verkin Institute for Low Temperature Physics and Engineering, NAS of Ukraine, 47, Lenin Avenue, 61103 Kharkov, Ukraine, and Department of Chemistry, University of Arizona, Tucson, Arizona 85721

Received: November 20, 2008; Revised Manuscript Received: March 2, 2009

In this work, we have used Raman spectroscopy and quantum chemical methods (MP2 and DFT) to study the interactions between nucleic acid bases (NABs) and single-walled carbon nanotubes (SWCNT). We found that the appearance of the interaction between the nanotubes and the NABs is accompanied by a spectral shift of the high-frequency component of the SWCNT G band in the Raman spectrum to a lower frequency region. The value of this shift varies from 0.7 to 1.3 cm^{-1} for the metallic nanotubes and from 2.1 to 3.2 cm^{-1} for the semiconducting nanotubes. Calculations of the interaction energies between the NABs and a fragment of the zigzag(10,0) carbon nanotube performed at the MP2/6-31++G(d,p)[NABs atoms]|6-31G(d)[nanotube atoms] level of theory while accounting for the basis set superposition error during geometry optimization allowed us to order the NABs according to the increasing interaction energy value. The order is: guanine (-67.1 kJ mol^{-1}) > adenine (-59.0 kJ mol^{-1}) > cytosine (-50.3 kJ mol^{-1}) ≈ thymine (-50.2 kJ mol^{-1}) > uracil (-44.2 kJ mol^{-1}). The MP2 equilibrium structures and the interaction energies were used as reference points in the evaluation of the ability of various functionals in the DFT method to predict those structures and energies. We showed that the M05, MPWB1K, and MPW1B95 density functionals are capable of correctly predicting the SWCNT-NAB geometries but not the interaction energies, while the M05-2X functional is capable of correctly predicting both the geometries and the interaction energies.

1. Introduction

Although the interactions between carbon nanotubes and small molecules have been studied with computational methods before (see, for example, ref 1 and papers cited therein), theoretical studies of the interactions between larger organic molecules, including the nucleic acid bases (NABs), and carbon surfaces have received less attention.[1−7] The main reason for this is the large size of the fragment of the carbon surface that needs to be used to correctly model the interaction between a single-walled carbon nanotube (SWCNT) and a biomolecule. Moreover, the stacked complexes, which are formed by organic molecules and SWCNTs, are predominantly stabilized by van der Waals forces, which require the application of computationally expensive quantum chemical methods for their correct description. Despite the need for a rather high-level treatment, the interactions between NABs and carbon nanotubes were investigated with the HF[2] method, and, as one may expect, this method, which does not account for the dispersion interactions, was unable to describe the NAB−nanotube stacked structures. Recently,[1] we studied the interactions between cytosine and nanotube surface fragments with different sizes (from $C_{38}H_{16}$ to $C_{120}H_{20}$) applying the DFT method with the new generation density functionals, MPWB1K, MPW1B95, M05, and M05-2X, and we showed that these functionals are able to correctly predict the stacked cytosine−nanotube structure. Wang and Bu have also studied the interaction between cytosine[3] and other nucleobases[4] and a small nanotube surface ($C_{24}H_{12}$) using the DFT (PW91LYP and MPWB1K functionals) and MP2 methods. The orientation of the cytosine molecule with respect to the nanotube surface they determined was different from the orientations we obtained using larger surface models in the calculations.[1] Most probably this happened because the fragment of the nanotube surface used by Wang and Bu was too small to allow the cytosine molecule to assume the most optimal position with respect to the surface. The interaction between NABs and a small-diameter (5,0) carbon nanotube was also studied using the LDA approximation by Gowtham et al.[5] Antony and Grimme studied noncovalent interactions of graphene with NABs and with hydrogen-bonded base pairs using the DFT-D method.[6] Also, Shtogun et al. considered the adsorption of adenine on the metallic SWCNT (6,6) and the adsorption of thymine on the semiconducting (8,0) SWCNT with nonspin-polarized LDA.[7] Recently Kar et al. studied interactions between small aromatic systems and SWCNT applying the MP2 theory.[8] They demonstrated that DFT (LDA or GGA) binding energies for $\pi-\pi$ stacking arrangements are underestimated, whereas dispersion-corrected methods (DFT-D) overestimate these binding energies.

As it is seen, most of the work on NAB−nanotube (or graphene) interactions has been performed using the DFT methods employing different functional. The outcome of that work was dependent on the type of functional used. Even if the interaction energy was calculated at the MP2 level of theory, the use of the DFT geometries in the calculations may have affected the results. It would be more useful if the geometries of the complexes were calculated at the MP2 level of theory. Such results would provide a reference to estimate the accuracy of the different density functional methods. Such reference calculations are carried out in the present work. They concern

* Corresponding author. E-mail: stepanian@ilt.kharkov.ua.
† NAS of Ukraine.
‡ University of Arizona.

10.1021/jp810205a CCC: $40.75
Published on Web 03/25/2009

NAB−nanotube and NAB−graphene complexes. The calculations employ different basis sets. This allows testing of how the quality of the basis sets affects the interaction energy. We paid special attention to the accounting of the basis set superposition error (BSSE). Usually the BSSE is corrected at the final stage of the calculation when the interaction energy is determined, but not in the optimization of the geometry of the complex. However, the BSSE may significantly influence the geometrical parameters, and thus, in the calculations performed in this work, we included BSSE in the geometry optimization. The reference MP2 results are used in this work to test the performance of the following density functionals: MPWB1K, MPW1B95, M05, M05-2X, PBE1KCIS, and B97-1.

2. Experimental Details

Sample Preparation. HiPCO CVD-produced SWCNTs were purified by controlled thermal oxidation followed by the HCl treatment.[9] The diameters of nanotubes were within 0.6−1.9 nm. NABs (adenine, guanine, and thymine) purchased from Sigma-Aldrich, Europe, were used in the experiment without preliminary purification. First, the SWCNTs and the mixtures of SWCNTs with the NABs (with weight ratio 1:2) in toluene (0.3 mg/mL) were subjected to an ultrasound sonication treatment (1 W, 44 kHz) for 50 min. After this preparatory step, suspensions of nanotubes and nanotubes with a NAB were deposited on the quartz substrate and dried under a stream of warm air.

Methods. The Raman experiments were performed in the quasi-backscattering configuration using the 632.8 nm (1.96 eV) light from a He−Ne laser. The laser power was focused onto a strip (~0.1 mm × 1 mm) to deliver the laser power density of 100 W/cm^2. The spectra were analyzed using a Raman double monochromator with the reverse dispersion of 3 Å/mm. The spectra were detected with a thermo-cooled CCD camera. The peak position of the G^+ band located in the spectral range between 1500−1630 cm^{-1} in nanotube films was determined with an accuracy no worse than 0.3 cm^{-1}. Such accuracy was achieved because the frequency positions of the plasma lines from the He−Ne laser in the vicinity of the G^+ band were used for the internal calibration of the spectrometer.

3. Computational Details

Methods. The geometries of the NAB−nanotube complexes were optimized at the MP2 and DFT levels of theory. In the DFT calculations, we used the following functionals: MPWB1K,[10−12] MPW1B95,[10−12] M05,[13] M05-2X,[13] PBE1KCIS,[14] and B97-1.[15] For the geometries optimized at the DFT level of theory, we also performed single-point MP2//DFT energy calculations. The counterpoise (CP) corrections were included in the MP2//DFT calculations of the interaction energies using the standard procedure.[16] For all NAB−nanotube complexes, we also performed BSSE-free geometry optimizations at the MP2 level of theory. In the BSSE-free optimization, the CP correction is accounted for in each step of the optimization.

Basis Sets. In this work, we used four different basis sets denoted as BS1, BS2, BS3, and BS4. To reduce the total number of the basis functions, we used the STO-3G basis for the terminal hydrogen atoms of the nanotube surface. For the nanotube carbons and for all NAB atoms, we used the standard double and triple split-valence basis sets, 6-31G and 6-311G, augmented with diffuse and polarization functions. The four basis sets used in the calculations are the following: BS1, 6-31G(d) [nanotube carbons], 6-31++G(d,p) [NABs]; BS2, 6-31+G(d) [nanotube carbons], 6-31++G(d,p) [NABs]; BS3, 6-311+G(d) [nanotube carbons], 6-311++G(d,p) [NABs]; BS4, 6-311+G(2d) [nanotube carbons], 6-311++G(2d,p) [NABs].

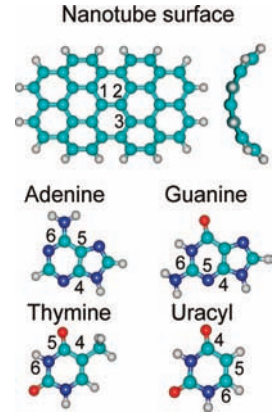

Figure 1. The structures of the zigzag(10,0) nanotube fragment and the NABs including atom numbering used in this work to describe the intermolecular and intramolecular structural parameters.

Models. The calculations were performed for complexes of NABs with fragments of the zigzag(10,0) nanotube and the planar graphene surface, which included 38 carbon atoms and 16 hydrogen atoms. Earlier we demonstrated[1] that this surface size is sufficient to correctly predict geometries and the interaction energies of NAB−nanotube complexes. The nanotube surface fragments, as well as the NABs considered in this study, are shown in Figure 1. The geometry of the fragment of the nanotube surface was determined in a two-step procedure. First, we fully optimized the structure of a 5-band zigzag(10,0) SWCNT terminated by hydrogen atoms. In the calculation, we used the DFT method with the B3LYP functional and the standard 3-21G basis set. Next, we cut out a fragment of the nanotube, terminated the dangling bonds with hydrogen atoms, and optimized the hydrogen positions at the B3LYP/3-21G level of theory while keeping the positions of the carbon atoms frozen. In all calculations of the complexes that followed, the geometry of the surface fragment was taken from that full optimization, and it was not optimized. All calculations reported in this work were performed using the Gaussian 03 program package.[17]

4. Results and Discussion

Raman Spectra. The Raman spectra of SWCNTs (1), SWCNT-thymine (2), SWCNT-guanine (3), and SWCNT-adenine (4) in the range of the tangential G-mode (1500−1630 cm^{-1}) are shown in Figure 2. On the whole, all of the spectra are similar, but a detailed spectral analysis reveals some small differences in the band positions and the intensities. In the analysis of the spectra, some peculiarities resulting from SWCNTs irradiation with the He−Ne laser should be taken into account. For example, a 1.96 eV excitation of nanotubes with diameters in the range of 0.6−1.9 nm gives rise to Raman bands, which can be assigned both to semiconducting and to metallic nanotubes.[18] Thus, the observed spectrum is a superposition of the two types of spectra.

The low-frequency component of the G band (in the range 1540 cm^{-1}) is wide and has an asymmetric form, which strongly broadens in the region of lower frequencies. As was shown,[19,20] the sloping lower-frequency front of the band is due to metallic nanotubes. The shape of such a band is well described by the Breit−Wigner−Fano (BWF) function ($I(\omega) = I_0\{1 + (\omega - \omega_0)/q\Gamma\}^2/\{1 + [(\omega - \omega_0)/\Gamma^2\}$, where I_0, ω_0, Γ, and q are the

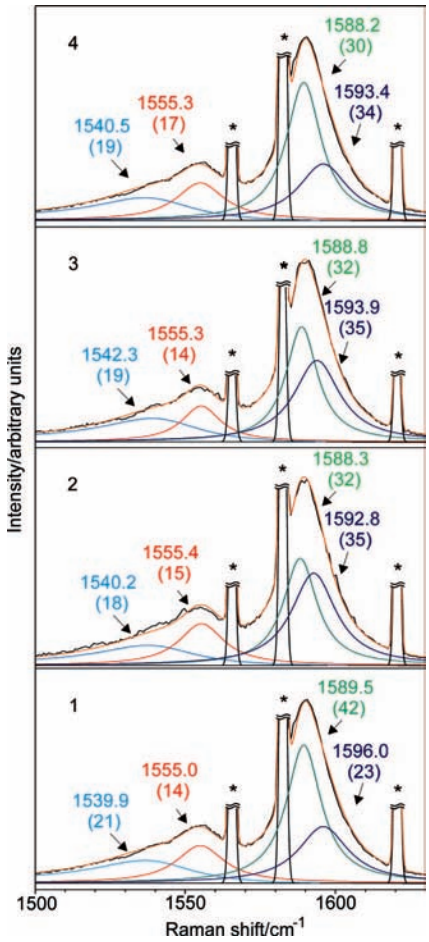

Figure 2. Raman spectra of pure SWCNTs (1), SWCNT-thymine (2), SWCNT-guanine (3), and SWCNT-adenine (4) in the range of the tangential G-mode. Each experimental spectrum (dashed curve) obtained with $\lambda_{exc} = 632.8$ nm laser light was fitted with a sum (dot lines) of one BWF function and three Lorentzians. The parameter $1/q$ of the BWF bands obtained for different samples was in the range of -0.12 to 0.18. The value of the band peak position and its area (in brackets) is indicated in the figure close to the band location. Peaks labeled "*" correspond to the plasma line of the laser.

intensity, the BWF peak frequency, the broadening parameter, and the asymmetry parameter, respectively.

The features in every experimental spectrum were fitted with a sum of three Lorentzians and one BWF function (Figure 2). As can be seen in Figure 2, the agreement between the calculated (broken line) and the experimental spectra is very good. As a result of the fitting, the peak positions, the integral intensities (area), and the full-widths corresponding to the half-maximum intensity levels were determined, and they are presented in Table 1. The peak position and its area for each band are shown in Figure 1 near the band position. Each spectral band was normalized so that the area of all bands became equal to 100. Two bands with peaks close to 1540 and 1590 cm^{-1} can be assigned to the metallic nanotubes and the other two bands to the semiconducting nanotubes.[20] The separation of the nanotubes in a bundle by nucleobases is accompanied by a decrease of the integral intensity of the BWF band in all nanotube−base samples. It is also accompanied by the diminution of the width of the G^+ bands for both the metallic and the semiconducting nanotubes. It should be noted that the ratio of the integrated intensities for the G bands associated with the metallic tubes and of those of the semiconducting tubes decreases from 1.7 for pristine SWCNTs to 0.96−1.04 in films with the NABs.

The intensity of the low-frequency component of the G-mode corresponding to the metallic nanotubes is very sensitive to the external surrounding and to the interaction between the tubes. In thick bundles, the intensity of the G-mode is high, and upon their splitting the band becomes less intensive.[21] In accordance with the theory,[22] the strong van der Waals interactions between metallic tubes enhance the coupling between the plasmon modes and the G-modes. As a result, the BWF band intensity increases.

The observed decreasing of the BWF band can be explained by the splitting of the nanotube bundles under the sonication treatment in toluene, and by adsorption of nitrogen bases on the surfaces of individual nanotubes. The adsorption prevents the aggregation of the tubes and formation of bundles after the deposition on the substrate.

The interaction between a nanotube and a nitrogen base is accompanied by a spectral shift of the high-frequency component of the G-band to a lower frequency region in comparison with the G-band position in the pristine SWCNTs spectrum. The value of this shift varies in the range between 0.7 and 1.3 cm^{-1} for the metallic nanotubes and between 2.1 and 3.2 cm^{-1} for the semiconducting nanotubes (Table 1). This downshift of the G-band frequency can be explained by a partial electron transfer from the NAB molecule to the nanotube surface. The magnitude of this charge transfer does not exceed a few percent of the charge of an electron.[18,23]

Structure of the NAB−Nanotube Dimers. For each NAB, we first determined all possible stable conformations of the NAB−nanotube complex. In this determination, we first selected six initial structures for each complex of a particular NAB with the nanotube fragment. These six structures differed in terms of the orientation of the NAB with respect to the nanotube surface. In all of these initial structures, NAB was placed 3.3 Å above the nanotube surface, and the NAB plane was set parallel to the surface. The six structures were then generated by rotating the NAB around its perpendicular axis in increments of 30°. Next, the six structures were used as starting points in geometry optimizations. These optimizations were performed at the MP2/BS1 (BSSE-free optimization), M05-2X/BS1, and MPWB1K/BS1 levels of theory. The calculations converged to three stable confirmations for each of the adenine−nanotube, guanine−nanotube, and uracil−nanotube complexes and to two stable conformations of the thymine−nanotube complex.

For the cytosine−nanotube complex, we performed additional calculations with a much smaller step of the angle between the base and the nanotube surface (5°). The calculations produced the same three stable structures of the complex as the calculations with the larger step (30°).[1] Detailed results of the calculations are collected in Table S1. The relatively small number of the possible structures of the NAB−nanotube complexes may be due to the high local symmetry of the carbon nanotube surface. It should be noted that in all equilibrium structures of NAB−nanotube complexes presented in this work there are no direct contacts between the NABs and the hydrogen atoms terminating the surface. Such direct contacts may noticeably influence both the structures and the interaction energies of the studied systems. Obviously, hydrogen−nucleobase interactions are absent in the pristine nanotubes. In our models, we had to include peripheral hydrogens to limit the size of the nanotube surface in the calculations.

The most stable conformations of each NAB are shown in Figure 3. All calculated conformations are presented in Figure S1. For the most stable conformer of each NAB−nanotube dimer, we also performed geometry optimizations at the M05/BS1, MPW1B95/BS1, B97-1, and PBE1KCIS/BS1 levels of

TABLE 1: Spectral Position (ν, cm^{-1}), Relative Area (S), and Full-Width ($\Delta\Gamma$, cm^{-1}) at Half-Maximum Intensity of BWF (1) and of Lorentzians (2−4) Used To Fit the Bands Associated with the G-Mode of the SWCNTs Obtained with the Laser Light with λ_{exc} = 632.8 nm[a]

	SWCNTs			SWCNTs:adenine			SWCNTs:guanine			SWCNTs:thymine		
N	ν	$\Delta\Gamma$	S	ν	$\Delta\Gamma$	S	ν	$\Delta\Gamma$	S	ν	$\Delta\Gamma$	S
1	1539.9	40.5	21	1540.5	39.8	19	1542.3	40.2	19	1540.2	39.6	18
2	1555.0	16.6	14	1555.3	19.5	17	1555.3	18.1	14	1555.4	18.3	15
3	1589.5	14.1	42	1588.2	12.8	30	1588.8	12.8	32	1588.3	13.6	32
4	1596.0	20.1	23	1593.4	16.5	34	1593.9	18.5	35	1592.8	18	35
M:S		1.7:1			0.96:1			1.04:1			1:1	

[a] M:S denotes the ratio of the total area of the G bands associated with the metallic nanotubes (1 + 3) and the semiconducting nanotubes (2 + 4).

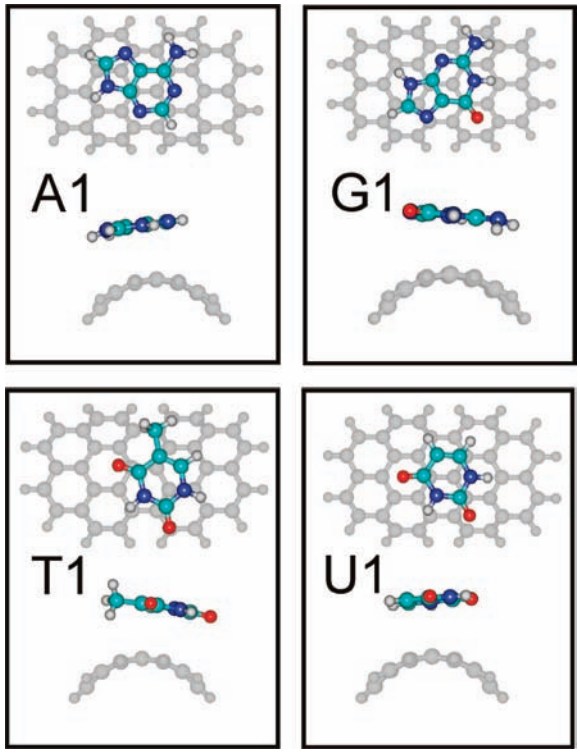

Figure 3. Top and side views of the most stable conformations of the NAB−nanotube complexes obtained in the M05-2X/BS1 calculations.

theory. In Table 2, we show the intermolecular parameters corresponding to the most stable conformations for each NAB (G1, A1, T1, and U1). These parameters describe the orientation of the NAB molecule with respect to the nanotube surface.

On the basis of the comparison of the MP2 and DFT intermolecular parameters presented in Table 2, we evaluated the performance of the different density functionals in predicting the NAB−nanotube geometries. This analysis allowed us to group the functionals into three sets dependent on the functional performance. The first group of functionals, M05-2X, MPWB1K, and MPW1B95, predict the geometries of the dimers in very good agreement with the MP2 geometries. As it is seen from Table 2, the DFT calculations with these functionals provide fairly accurate values of the distances between the NABs and the nanotube surface. The average difference between the MP2 and DFT intermolecular distances is about 0.02 Å, and the maximum difference does not exceed 0.05 Å. The bond and dihedral angles calculated with the M05-2X, MPWB1K, and MPW1B95 functionals are also in very good agreement with the MP2 values. The average differences between the MP2 and DFT bond angles and the dihedral angles are 0.07° and 1.4°, respectively, and the maximum differences do not exceed 2° and 3°, respectively. Thus, we may conclude that the M05-2X, MPWB1K, and MPW1B95 density functionals are very effective in predicting the structures of stacked complexes of carbon nanotubes with π-conjugated organic molecules.

The PBE1KCIS and B97-1 functionals belonging to the second group are rather ineffective in predicting the NAB−nanotube structures. As seen in Table 2, these functionals overestimate the intermolecular distances for the adenine, guanine, and cytosine complexes with the nanotube surface by 0.4−0.5 Å in comparison to the MP2 distances. Moreover, these functionals fail to predict the stacked structures for the uracil−nanotube and thymine−nanotube complexes. For these two bases, the geometry optimizations of the complexes converged to almost perpendicular structures with the angles between the NAB planes and the nanotube surface of 60−80°.

Finally, the M05 functional, belonging by itself to the third group of functionals, shows the performance that falls between the performances of the functional in the two groups mentioned above. This functional is able to predict the stacked structure for all of the NAB−nanotube complexes, but, similarly to the B97-1 and PBE1KCIS functionals, it overestimates the intermolecular distance between the NABs and the nanotube surface, although the average difference between the M05 and MP2 geometries is only about 0.26 Å.

An accurate prediction of the intermolecular parameters for the NAB−nanotube complexes is an important test of the DFT functionals because these parameters (most importantly, the intermolecular distance) significantly influence the NAB−nanotube interaction energies.

Wang and Bu studied interactions between NABs and nanotube surfaces employing the MPWB1K functional.[3,4] The number and structure of the NAB−nanotube conformers found by them are different from our results. Most probably, it happens due to the smaller size of the nanotube fragment used in refs 3 and 4, which included only 24 carbon atoms. This model is too small to avoid direct interactions between NABs and the peripheral hydrogen atoms of the nanotube fragment. The interaction should change the potential energy surface for the NAB−nanotube complexes.

Interaction Energies. The interaction energies obtained in the MP2/BS1 and MP2/BS1//DFT/BS1 calculations are presented in Table 3 for guanine and adenine and in Table 4 for cytosine, thymine, and uracil. The comparison of the DFT and MP2//DFT (the "MP2//DFT" notation means that the energy was calculated at the MP2 level of theory for the geometry obtained at the DFT level of theory) interaction energies is also shown in Figure 4. In Figure 5, the MP2//DFT interaction energies are compared to the MP2//MP2 interaction energies obtained in the BSSE-free geometry optimizations.

First, upon examining the results in Tables 3 and 4 and Figures 4 and 5, one can notice the poor performance of the

TABLE 2: Intermolecular Parameters (*R* is the Intermolecular Distance in Å; *A* is the Bond Angle in degrees; *D* is the Dihedral Angle in degrees) Calculated for the Most Stable Conformations of the NAB−Nanotube Complexes at the DFT/BS1 and MP2/BS1 Levels of Theory[a]

	method	G1	A1	C1[b]	T1	U1
R_{1-4}	MP2[c]	3.132	3.168	3.194	3.206	3.273
	M05-2X	3.117	3.186	3.141	3.209	3.237
	MPWB1K	3.139	3.175	3.183	3.221	3.288
	MPW1B95	3.137	3.172	3.177	3.219	3.285
	M05	3.388	3.457	3.436	3.468	3.445
	PBE1KCIS	3.516	3.608	3.624	NS[d]	NS[d]
	B97-1	3.443	3.591	3.571	NS[d]	NS[d]
A_{1-4-5}	MP2[c]	89.6	92.0	92.8	80.2	86.1
	M05-2X	89.3	91.5	92.4	80.4	85.3
	MPWB1K	88.7	91.3	93.4	81.2	85.5
A_{2-1-4}	MP2[c]	88.1	91.0	89.7	95.6	92.9
	M05-2X	87.5	91.6	90.8	96.5	94.0
	MPWB1K	86.2	90.7	88.1	96.3	94.2
$D_{1-4-5-6}$	MP2[c]	−92.4	−88.3	−85.2	84.7	−84.2
	M05-2X	−91.5	−86.2	−86.7	84.5	−82.0
	MPWB1K	−91.5	−87.0	−89.5	82.9	−82.3
$D_{2-1-4-5}$	MP2[c]	66.0	62.3	60.1	36.4	57.0
	M05-2X	64.2	62.7	60.8	37.9	57.7
	MPWB1K	63.7	61.9	57.9	37.5	59.1
$D_{3-2-1-4}$	MP2[c]	102.0	107.2	101.4	98.8	102.7
	M05-2X	103.3	108.3	98.5	98.8	102.0
	MPWB1K	100.5	108.4	101.6	96.5	99.6

[a] Atom numbering is shown in Figure 1. [b] From ref 1. [c] BSSE-free optimization. [d] Nonstacked structure.

TABLE 3: Interaction Energies (kJ mol^{-1}) between Adenine, Guanine, and Zigzag(10,0) SWCNT Calculated at the DFT and MP2 Levels of Theory

	adenine			guanine		
method	A1	A2	A3	G1	G2	G3
MPWB1K/BS1	−39.6	−37.7	−35.9	−49.9	−50.5	−44.2
MPW1B95/BS1	−38.1			−48.1		
PBE1KCIS/BS1	−27.3			−35.6		
B97-1/BS1	−29.8			−37.1		
M05/BS1	−37.1			−45.1		
M05-2X/BS1	−49.5	−48.8	−44.2	−61.2	−59.5	−54.0
MP2/BS1//MPWB1K/BS1	−56.3	−54.1	−49.5	−65.4	−62.1	−56.7
MP2/BS1//MPW1B95/BS1	−56.6			−65.2		
MP2/BS1//PBE1KCIS/BS1	−46.5			−52.1		
MP2/BS1//B97-1/BS1	−47.4			−55.4		
MP2/BS1//M05/BS1	−50.4			−59.0		
MP2/BS1//M05-2X/BS1	−57.2	−58.1	−51.2	−65.8	−62.1	−58.1
MP2/BS1[a]	−59.0			−67.1		
MP2/BS2//M05-2X/BS1	−64.1			−71.3		
MP2/BS3//M05-2X/BS1	−71.2			−77.3		
MP2/BS4//M05-2X/BS1	−77.2			−85.7		

[a] BSSE-free optimization.

PBE1KCIS and B97-1 functionals manifested in a significant difference between the interaction energies produced by these functionals and the MP2 interaction energies. As it is also seen, even for the stacked NAB−nanotube dimers, these two functionals significantly underestimate both of the interaction energies in comparison to the MP2 results (note that the structures of the uracil−nanotube and thymine−nanotube dimers calculated with the PBE1KCIS and B97-1 functional are not stacked). The difference between the DFT and MP2 interaction energies calculated for the guanine, adenine, and cytosine complexes with the nanotube is, on average, equal to about 30 kJ mol^{-1}, and the difference between MP2//DFT and MP2 interaction energies is about 10 kJ mol^{-1}. Taking into account that the PBE1KCIS and B97-1 functionals are unable to reproduce the stacked structures for the uracil−nanotube and thymine−nanotube van der Waals complexes, we conclude that these functionals should not be used to investigate these types of complexes.

Three other functionals (MPWB1K, MPW1B95, and M05) tested in this work produced reasonably accurate interaction energies for all studied systems. The average differences between the DFT and MP2 interaction energies are 11.8, 20.9, and 21.9 kJ mol^{-1} for the MPWB1K, MPW1B95, and M05 functionals, respectively, while the average differences between the MP2//DFT and MP2 interaction energies are 1.9, 1.9, and 6.1 kJ mol^{-1} for the MPWB1K, MPW1B95, and M05 functionals, respectively. At the same time, the M05-2X functional demonstrates an excellent performance in predicting the interaction energies; the average difference between the M05-2X and MP2 interaction energies is only 3.6 kJ mol^{-1}, and the average difference between the MP2//M05-2X and MP2 interaction energies is only 1.0 kJ mol^{-1}. This clearly demonstrates that the M05-2X functional is a viable alternative to the MP2 method in predicting structures of stacked complexes.

The MP2/BS1 interaction energies presented in Tables 3 and 4 were obtained using BSSE-free geometry optimization. To

TABLE 4: Interaction Energies (kJ mol^{-1}) between Thymine, Cytosine, Uracil, and Zigzag(10,0) SWCNT Calculated at the DFT and MP2 Levels of Theory

	thymine		cytosine				uracil	
method	T1	T2	C1	C2	C3	U1	U2	U3
MPWB1K/BS1	−40.9	−41.0	−39.9[c]	−36.5	−35.1	−35.1	−30.1	−34.0
MPW1B95/BS1	−39.7		−38.5			−33.7		
PBE1KCIS/BS1	−31.6[b]	−28.7			−32.6[b]			
B97-1/BS1	−32.1[b]	−30.2			−28.6[b]			
M05/BS1	−37.6		−36.4[c]			−33.4		
M05-2X/BS1	−49.6	−48.0	−48.7[c]	−45.1	−45.3	−43.6	−43.4	−42.2
MP2/BS1//MPWB1K/BS1	−48.7	−45.7	−49.6[c]	−45.4	−45.3	−42.2	−38.9	−40.1
MP2/BS1//MPW1B95/BS1	−48.7		−49.4			−42.3		
MP2/BS1//PBE1KCIS/BS1	−39.4[b]	−41.0			−30.6[b]			
MP2/BS1//B97-1/BS1	−35.3[b]	−41.6			−35.7[b]			
MP2/BS1//M05/BS1	−45.2		−45.2[c]			−39.8		
MP2/BS1//M05-2X/BS1	−49.3	−45.8	−49.6[c]	−45.7	−46.2	−43.5	−41.5	−40.4
MP2/BS1[a]	−50.2		−50.3[c]			−44.2		
MP2/BS2//M05-2X/BS1	−54.7		−55.1			−48.7		
MP2/BS3//M05-2X/BS1	−59.2		−60.7			−52.1		
MP2/BS4//M05-2X/BS1	−65.5		−65.6			−58.3		

[a] BSSE-free optimization. [b] Nonstacked structure. [c] From ref 1.

demonstrate how important is the accounting for the BSSE during optimization, we performed additional calculations of the cytosine−nanotube and uracil−nanotube complexes. It these calculations, geometry of the most stable conformations C1 and U1 was optimized using conventional procedure, and the BSSE correction was accounted for after optimization. The interaction energies obtained in these calculations were −42.5 and −37.9 kJ mol^{-1} for the C1 and U1 complexes, respectively. As it is seen, these values are significantly different from the MP2/BS1 interactions energies presented in Tables 3 and 4. We should conclude that neglecting the BSSE correction during optimization leads to significant underestimating of the interaction energies (in absolute values). We also found that neglecting the BSSE correction significantly underestimates the intermolecular distances between NAB and nanotube: by 0.238 and 0.305 Å for the C1 and U1 complexes, respectively. These results clearly demonstrate that MP2 calculations of stacked systems should be performed while accounting for the BSSE correction during optimization.

The interaction energies calculated for all NABs (Tables 3 and 4) at the MP2/BS1 level of theory allow us to order them according to the increasing stabilty of the NAB−nanotube complex. This order is the following: guanine (−67.1 kJ mol^{-1}) > adenine (−59.0 kJ mol^{-1}) > cytosine (−50.3 kJ mol^{-1}) ≈ thymine (−50.2 kJ mol^{-1}) > uracil (−44.2 kJ mol^{-1}). The order demonstrates that there is a dependency between the size of the NAB molecule and the interaction energy with the nanotube fragment. The comparison of the interaction energies with the NAB nanotube intermolecular distances clearly shows a correlation between (Table 2) these parameters. In going from guanine to uracil, the intermolecular distances increase from 3.132 to 3.273 Å. This trend reflects the trend observed for the interaction energies. As the cytosine and thymine nanotube dimers both have similar interaction energies (−50.3 and −50.2 kJ mol^{-1}, respectively), their intermolecular distances are also similar (3.194 and 3.206 Å, respectively). The stability order calculated at the MP2//DFT level of theory is identical to the one calculated at the MP2 level of theory (Figure 5). As seen from Figure 5, the MP2//M05-2X, MP2//MPWB1K, and MP2//MPW1B95 interaction energies are almost identical to the MP2//MP2 interaction energies. This confirms the ability of these functionals to correctly predict the geometries of the stacked complexes. As mentioned above, the M05 functional overestimates the intermolecular distances between the NABs and the nanotube fragment by 0.26 Å on average. As seen from Figure 4, this inaccuracy leads to lower MP2//M05 interaction energies as compared to the MP2//MP2 interaction energies.

An analysis of the calculated interaction energies demonstrates that all functionals underestimate the interaction energies for purine bases, guanine, and adenine, with respect to the interaction energies for the pyrimidine bases, cytosine, thymine, and uracil. Hence, the difference between the MP2//MP2 and MP2//DFT interaction energies calculated for the dimers of the pyrimidine bases is smaller than the corresponding difference for the purine bases. For example, the M05-2X interaction energies calculated for the pyrimidine bases are almost identical to the MP2//M05-2X energies. At the same time, the interaction energies calculated by the M05-2X and MP2//M05-2X methods for the adenine−nanotube and guanine−nanotube dimers differ by 7.5 and 4.6 kJ mol^{-1}, respectively. As a result, the stability order obtained at the DFT level of theory with all of the functionals tested here is different from the order obtained at the MP2 or MP2//DFT level of theory. This is clearly seen in Figure 4.

The NAB−nanotube interaction energies were obtained in this work for dimers formed by NABs with a fragment of the zigzag(10,0) SWCNT. Increasing the diameter of the nanotube leads to flattening of the nanotube surface, which in turn leads to increased contact between the NAB and the surface. This should lead to an increase in the interaction energy. We demonstrated this effect in an earlier work where we showed that as the diameter of the nanotube increases the interaction energy between the cytosine and nanotube surface also increases. Eventually the interaction energy approaches the result obtained for the cytosine−graphene complex.[1] The interaction energy for all other NABs should also increase with the increase of the nanotube diameter, and the interaction energy of NABs with planar grapheme should provide an upper limit to this interaction energy. To test that, we performed additional calculations for the NABs complexed with a fragment of the planar graphene surface with the same size as the fragment of the nanotube surface shown in Figure 2. The geometries of the complexes were optimized at the M05-2X/BS1 level of theory, and the interaction energies were calculated at the M05-2X/BS1 and MP2/BS1//M05-2X/BS1 levels of theory. The results are presented in Table 5 and Figure 6.

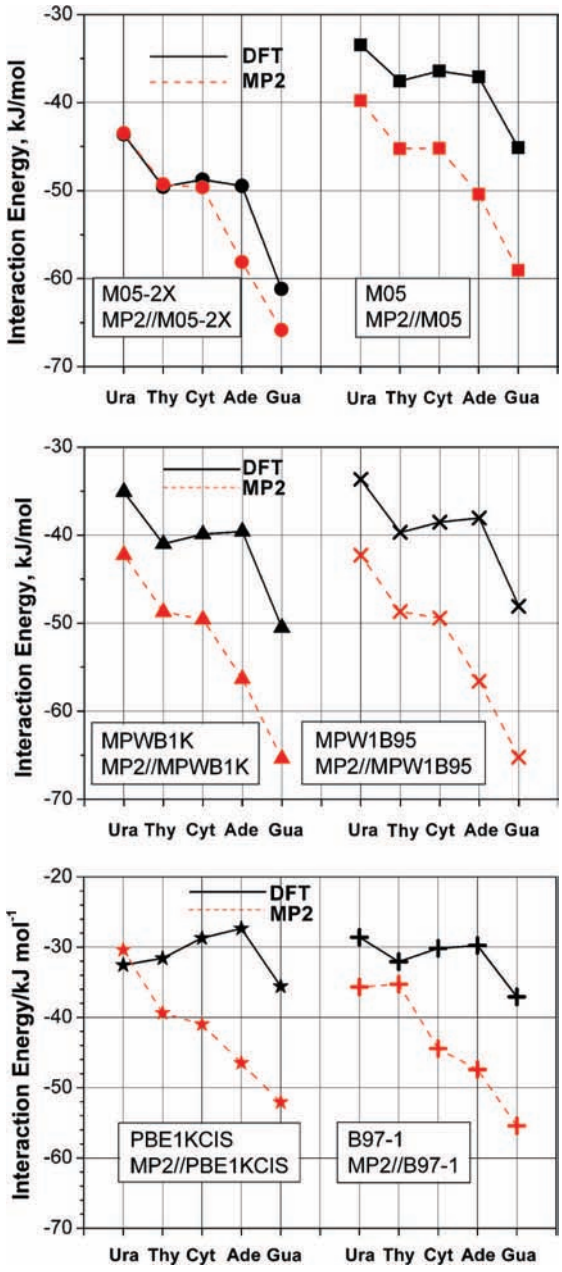

Figure 4. The interaction energies calculated at the DFT/BS1 and MP2/BS1//DFT/BS1 levels of theory for the most stable NAB−nanotube conformers.

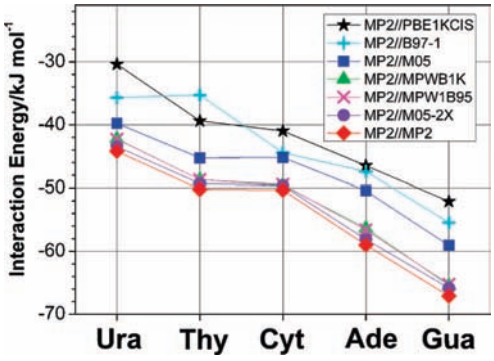

Figure 5. Comparison of the MP2/BS1//DFT/BS1 and MP2/BS1 interaction energies calculated for the most stable NAB−nanotube conformers.

As the results show, there is a dependency between the size of the NAB and the difference between the NAB nanotube and

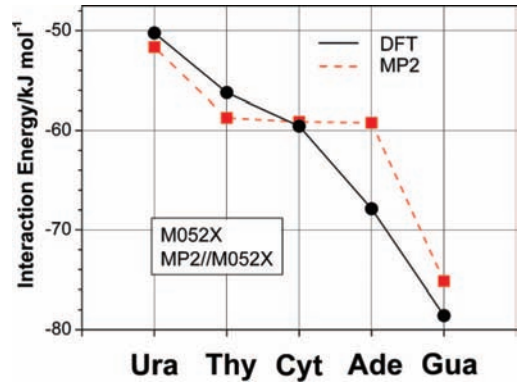

Figure 6. Interaction energies calculated at the M05-2X/BS1 and MP2/BS1//M05-2X/BS1 levels of theory for the most stable NAB−graphene conformers.

TABLE 5: Interaction Energies (IE, kJ mol^{-1}) between Nucleic Acid Bases and Planar Graphene Surface Calculated at the M05-2X/BS1 and MP2/BS1//M05-2X/BS1 Levels of Theory and Difference between the Interaction Energies (ΔIE, kJ mol^{-1}) of the NABs with Planar Graphene and with Zigzag(10,0) Nanotube Surfaces

	M05-2X		MP2//M05-2X	
conformer	IE	ΔIE	IE	ΔIE
G1	−75.2	14.0	−78.6	12.8
A1	−59.2	9.7	−67.9	10.7
T1	−58.7	9.1	−56.2	6.9
C1	−59.1	10.4	−59.6	10.0
U1	−51.7	8.1	−50.2	6.7

NAB−graphene interaction energies. The largest interaction energy corresponds to the largest NAB, guanine, and the smallest interaction energy corresponds to the smallest NAB, uracil. Both M05-2X/BS1 and MP2/BS1//M05-2X/BS1 levels of theory agree on that. It is interesting that the interaction-energy increase found for the complexes involving cytosine is larger than that found for the thymine (by 1.3 and 3.1 kJ mol^{-1} at the M05-2X and MP2//M05-2X levels of theory, respectively). This results in a change of the NAB stability order (G > A > C ≈ T > U) calculated at the MP2 level of theory. The interaction of cytosine with the planar graphene fragment is stronger than the thymine−graphene interaction as it is seen in Figure 6. The MP2 interaction energies calculated for the NAB−graphene complexes allow us to write the following stability order: G > A > C > T > U. We should also note that the interaction energy increase found for the NABs with an amino group (guanine, adenine, cytosine) is larger than the energy for the NABs without that group (thymine and uracil).

To compare the influence of the different NAB side groups on the interaction energies, we analyzed the results obtained for adenine and guanine complexes with the nanotube and graphene fragments. We also performed additional calculations of the interaction energies at the M05-2X/BS1 and MP2/BS1//M05-2X/BS1 levels of theory for purine, 2-aminopurine, 2-oxopurine, and 6-oxopurine (hypoxanthine). The results obtained for the most stable conformations of these systems are presented in Figure 7.

The lowest interaction energy was found for unsubstituted purine−nanotube dimers, −46.0 and −52.0 kJ mol^{-1} at the M05-2X/BS1 and MP2/BS1//M05-2X/BS1 levels of theory, respectively. The adenine (6-aminopurine)−nanotube complex is by 3.5 (M05-2X) and 5.2 kJ mol^{-1} (MP2//M05-2X) more stable than the unsubstituted purine−nanotube complex. At the same time, the complexes of the 2-aminopurine nanotube

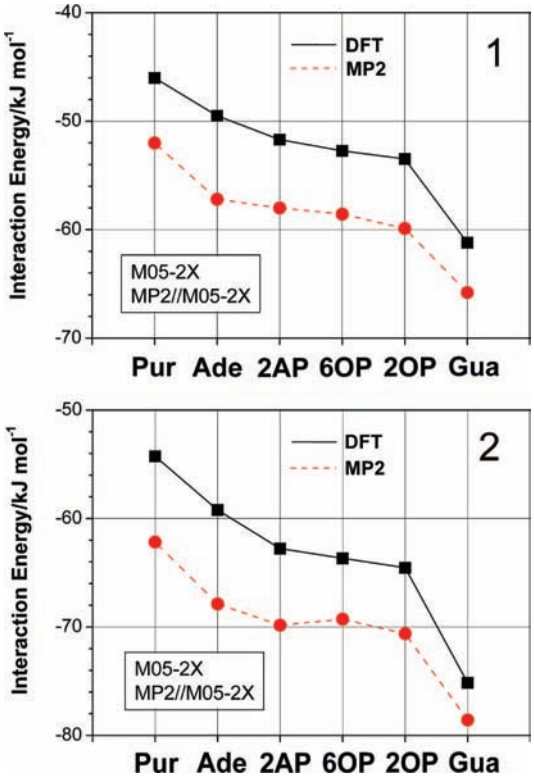

Figure 7. Interaction energies calculated at the M05-2X/BS1 and MP2/BS1//M05-2X levels of theory for the complexes of the purine, 6-oxopurine, 2-oxopurine, 2-aminopurine, adenine, and guanine with fragments of the zigzag(10,0) SWCNT (1) and graphene (2) surfaces.

complex are more stable than the purine−nanotube complexes by 5.7 (M05-2X) and 6.0 kJ mol^{-1}(MP2//M05-2X). It demonstrates that the 2-aminopurine−nanotube complexes are more stable than the adenine (6-aminopurine)−nanotube complexes. This effect may be due to the difference between the 2-aminopurine and adenine (6-aminopurine) structures. In adenine, the NH_2 group is located perpendicularly to the longest cross section of the molecule, but the 2-aminopurine molecule has a larger "footprint". Thus, the contact between the 2-aminopurine and the nanotube surface is larger in this case than for the adenine, and this results in the stronger interaction.

Impact of Basis Sets. The interaction energies and geometries calculated here were obtained with the BS1 basis set. This basis set should be considered a medium size set for the nanotube carbons. The limited size of the BS1 basis sets may have influenced the calculated NAB−nantoube interaction energies. To elucidate how an improvement of the basis set may influence the interaction energies and the relative stabilities of the NAB−nanotube complexes, we recalculated the interaction energies at the MP2//M05-2X level of theory with the BS2, BS3, and BS4 basis sets. The results of the calculations are shown in Figure 8.

The results demonstrate two important features. As one may expect, increasing the basis set leads to an increase of the interaction energies. The magnitude of this increase is very similar for all NABs. As a result, the relative stabilities of the complexes are virtually unchanged by the increase of the basis set size. It means that the stability order for the NAB−nanotube interactions does not depend on the quality of the basis set (for the basis sets used).

Larger Nanotube Model. The interaction energies presented in this work were obtained for the complexes of the NABs with

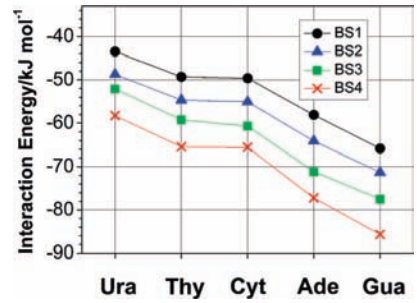

Figure 8. Interaction energies of the complexes of the most stable NAB−nanotube conformers calculated at the MP2//M05-2X level of theory with different basis sets.

a fragment of the SWCNT with a certain size ($C_{38}H_{16}$). Earlier[1] we showed that further increase of the fragment (to $C_{120}H_{20}$, which was the 5-band fragment of the full zigzag(10,0) SWCNT) does not significantly change the interaction energies. Thus, the interaction energies of cytosine with the $C_{38}H_{16}$ and $C_{120}H_{20}$ nanotube fragments were different only by 0.2 kJ mol^{-1}. These comparative calculations were performed for identical positions of cytosine with respect to the nanotube surface. This shows that the size of the nanotube surface model used here is sufficient for an accurate prediction of the interaction energies. However, there is another possible source of inaccuracy in the calculations. It is the freezing of the nanotube fragment structure during the optimization of the geometry of the complex. It is interesting to examine how the relaxing of the nanotube fragment would influence the interaction energies. This freezing could not have been avoided because relaxing the nanotube fragment structure would lead to flattening of the fragment. Thus, the only possible way to account for the effect of the freezing is to perform a full optimization of an NAB complex with a cylindrical fragment of the SWCNT. We performed such an optimization at the M05-2X/BS1 level of theory for the complex of a cytosine complex with 5-band long zigzag(10,0) nanotube terminated with hydrogen atoms. The resulting structure of the complex is shown in Figure S2. We found that the changes in both the geometry and the interaction energy of the complex are negligible in comparison with those quantities determined for the smaller nanotube fragment used throughout this work.

The interaction energies calculated for the cytosine complexes (conformer C1) with the $C_{38}H_{16}$ and $C_{120}H_{20}$ (we used both the frozen structure and the optimized structure) nanotube fragments are −48.7, −48.9, and −49.3 kJ mol^{-1}, respectively. The last two energies show that optimization of the nanotube fragment results in an increase of the interaction energy by only 0.4 kJ mol^{-1}. The structures of the complexes with the optimized and nonoptimized fragments are very similar. The distance between cytosine and the nanotube surface decreases by only 0.002 Å as a result of the optimization of the surface. Changes of the nanotube structure are negligible. Because of the full optimization, the change of the interaction energy of the cytosine nanotube complex is only 0.4 kJ mol^{-1}. Thus, it is clear that not optimizing the nanotube surface has almost no effect on the interaction energies and the geometries of the complexes considered in this work.

5. Conclusions

In the present work, the interaction between nucleic acid bases and carbon SWCNTs has been investigated using the MP2 and DFT methods and with the Raman spectroscopy. Analysis of the Raman spectra of pure SWCNTs and SWCNTs doped with

NABs shows that the NAB nanotube interactions cause a spectral down-shift of the high-frequency component of the G band of the SWCNTs. The shift varies between 0.7 and 1.3 cm^{-1} for the metallic nanotubes and between 2.1 and 3.2 cm^{-1} for the semiconducting nanotubes. We found that the ratio of the integrated intensities for the G bands associated with the metallic tubes and of those of the semiconducting tubes decreases from 1.7 for pristine SWCNTs to 0.96−1.04 in films with the NABs.

The geometry optimizations of the NAB−nanotube complexes performed with the DFT and MP2 methods produced three stable conformations for each of the adenine−nanotube, guanine−nanotube, and uracil−nanotube complexes and two stable conformations for the thymine−nanotube complex. The calculated interaction energies allow us to order the NAB−nanotube and NAB−graphene complexes according to their stabilities: guanine (−67.1 kJ mol^{-1}) > adenine (−59.0 kJ mol^{-1}) > cytosine (−50.3 kJ mol^{-1}) ≈ thymine (−50.2 kJ mol^{-1}) > uracil (−44.2 kJ mol^{-1}) (using the MP2/BS1 interaction energies); and guanine (−78.6 kJ mol^{-1}) > adenine (−67.9 kJ mol^{-1}) > cytosine (−59.6 kJ mol^{-1}) > thymine (−56.2 kJ mol^{-1}) > uracil (−50.2 kJ mol^{-1}) (using the MP2/BS1//M05-2X/BS1 interaction energies).

The comparison of the interaction energies and the geometries of the NAB−nanotube fragment complexes obtained using the BSSE-free MP2 geometry optimizations and using MP2 single-point calculations with the DFT geometries allowed us to evaluate the performance of various density functionals. The new-generation functional, M05-2X, was found to produce very accurate interaction energies and geometries of the complexes. The MPWB1K and MPW1B95 density functionals predicted the geometries of the complexes in close agreement with those obtained at the MP2 level of theory. However, these functionals underestimated the interaction energies. The M05 functional predicted stable stacked structures for all NAB−nanotube complexes, but it overestimated the NAB−nanotube distances and significantly underestimated the interaction energies. Last, the PBE1KCIS and B97-1 functionals failed to predict stacked structure for nanotube complexes of two NABs, uracil and thymine.

This study shows that stacked complexes formed by organic molecules with the carbon surface can be effectively studied with the MP2//M05-2X and M05-2X approaches. This is encouraging because these approaches are computationally much less expensive than the lowest-level ab initio alternative, the MP2 method.

Acknowledgment. We are in debt to the Center for Computing and Information Technology at the University of Arizona and to the Computational Center at the Institute for Low Temperature Physics and Engineering for a generous allotment of the computational resources used in this work. We are grateful to Dr. U. Dettlaff-Weglikowska (Max-Planck-Institute for Solid State Research) for purified SWCNT.

Supporting Information Available: Full Gaussian citation. Table S1. Figures S1 and S2. This material is available free of charge via the Internet at http://pubs.acs.org.

References and Notes

(1) Stepanian, S. G.; Karachevtsev, M. V.; Glamazda, A. Yu.; Karachevtsev, V. A.; Adamowicz, L. Stacking interaction of cytosine with carbon nanotubes: MP2, DFT and Raman spectroscopy study. *Chem. Phys. Lett.* **2008**, *459*, 153–158.

(2) Das, A.; Sood, A. K.; Maiti, P. K.; Das, M.; Varadarajan, R.; Rao, C. N. R. Binding of nucleobases with single-walled carbon nanotubes: Theory and experiment. *Chem. Phys. Lett.* **2008**, *453*, 266–273.

(3) Wang, Y. X.; Bu, Y. X. Noncovalent interactions between cytosine and SWCNT: Curvature dependence of complexes via $\pi\cdots\pi$ stacking and cooperative $CH\cdots\pi/NH\cdots\pi$. *J. Phys. Chem. B* **2007**, *111*, 6520–6526.

(4) Wang, Y. Theoretical evidence for the stronger ability of thymine to disperse SWCNT than cytosine and adenine: self-stacking of DNA bases vs their cross-stacking with SWCNT. *J. Phys. Chem. C* **2008**, *112*, 14297–14305.

(5) Gowtham, S.; Scheicher, R. H.; Pandey, R.; Karna, S. P.; Ahuja, R. First-principles study of physisorption of nucleic acid bases on small-diameter carbon nanotubes. *Nanotechnology* **2008**, *19*, 125701(6).

(6) Antony, J.; Grimme, S. Structures and interaction energies of stacked graphene-nucleobase complexes. *Phys. Chem. Chem. Phys.* **2008**, *10*, 2722–2729.

(7) Shtogun, Y. V.; Woods, L. M.; Dovbeshko, G. I. Adsorption of adenine and thymine and their radicals on single-wall carbon nanotubes. *J. Phys. Chem. C* **2007**, *111*, 18174–18181.

(8) Kar, T.; Bettinger, H. F.; Scheiner, S.; Roy, A. K. Noncovalent $\pi-\pi$ stacking and CH---π interactions of aromatics on the surface of single-wall carbon nanotubes: an MP2 study. *J. Phys. Chem. C* **2008**, *112*, 20070–20075.

(9) Dettlaff-Weglikowska, U.; Benoit, J.-M.; Chiu, P.-W.; Graupner, R.; Lebedkin, S.; Roth, S. Chemical functionalization of single walled carbon nanotubes. *Curr. Appl. Phys.* **2002**, *2*, 497–501.

(10) Zhao, Y.; Truhlar, D. G. Hybrid meta density functional theory methods for thermochemistry, thermochemical kinetics, and noncovalent interactions: The MPW1B95 and MPWB1K models and comparative assessments for hydrogen bonding and van der Waals interactions. *J. Phys. Chem. A* **2004**, *108*, 6908–6918.

(11) Becke, A. D. Density-functional thermochemistry. IV. A new dynamic correlation functional and implications for exact-exchange mixing. *J. Chem. Phys.* **1996**, *104*, 1040–1046.

(12) Adamo, C.; Barone, V. Exchange functionals with improved long-range behavior and adiabatic connection methods without adjustable parameters: the mPW and mPW1PW models. *J. Chem. Phys.* **1998**, *108*, 664–675.

(13) Zhao, Y.; Schultz, N. E.; Truhlar, D. G. Design of density functionals by combining the method of constraint satisfaction with parametrization for thermochemistry, thermochemical kinetics, and noncovalent interactions. *J. Chem. Theory Comput.* **2006**, *2*, 364–382.

(14) Zhao, Y.; Truhlar, D. G. Benchmark databases for nonbonded interactions and their use to test Density Functional Theory. *J. Chem. Theory Comput.* **2005**, *1*, 415–432.

(15) Hamprecht, F. A.; Cohen, A. J.; Tozer, D. J.; Handy, N. C. Development and assessment of new exchange-correlation functionals. *J. Chem. Phys.* **1998**, *109*, 6264–6271.

(16) Boys, S. F.; Bernardi, F. The calculation of small molecular interactions by the differences of separate total energies. Some procedures with reduced errors. *Mol. Phys.* **1970**, *19*, 553–566.

(17) Frisch, M. J.; *Gaussian 03*, revision E.01; Gaussian, Inc.: Pittsburgh, PA, 2004.

(18) Karachevtsev, V. A.; Glamazda, A. Yu.; Dettlaff-Weglikowska, U.; Leontiev, V. S.; Mateichenko, P. V.; Roth, S.; Rao, A. M. Spectroscopic and SEM studies of SWNTs: Polymer solutions and films. *Carbon* **2006**, *44*, 1292–1297.

(19) Kataura, H.; Kumazawa, Y.; Maniwa, Y.; Umezu, I.; Suzuki, S.; Ohtsuka, Y.; Achiba, Y. Optical properties of single-wall carbon nanotubes. *Synth. Met.* **1999**, *103*, 2555–2558.

(20) Dresselhaus, M. S.; Eklund, P. C. Phonons in carbon nanotubes. *Adv. Phys.* **2000**, *49*, 705–814.

(21) Kempa, K. Gapless plasmons in carbon nanotubes and their interactions with phonons. *Phys. Rev. B* **2002**, *66*, 195406(5).

(22) Jiang, C. Y.; Kempa, K.; Zhao, J. L.; Schlech, U.; Kolb, U.; Basche, T.; Burghard, M.; Mews, A. Strong enhancement of the Breit-Wigner-Fano Raman line in carbon nanotube bundles caused by plasmon band formation. *Phys. Rev. B* **2002**, *66*, 161404(4).

(23) Wise, K. E.; Park, C.; Siochi, E. J.; Harrison, J. S. Stable dispersion of single wall carbon nanotubes in polyimide: The role of noncovalent interactions. *Chem. Phys. Lett.* **2004**, *391*, 207–211.

JP810205A